Weather and Climate Extremes 44 (2024) 100684

Contents lists available at ScienceDirect

Weather and Climate Extremes

journal homepage: www.elsevier.com/locate/wace

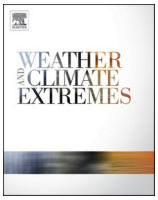

Mid-century climate change impacts on tornado-producing tropical cyclones

Dakota C. Forbis [a,*], Christina M. Patricola [a,b], Emily Bercos-Hickey [b], William A. Gallus Jr. [a]

[a] Department of Geological and Atmospheric Sciences, Iowa State University, 716 Farm House Ln, Ames, IA, 50011, USA
[b] Climate and Ecosystem Sciences Division, Lawrence Berkeley National Laboratory, 1 Cyclotron Rd, Berkeley, CA, 94720, USA

ARTICLE INFO

Keywords:
Climate change
Tropical cyclones
Tornadoes
Severe weather
Convective-allowing model
Numerical weather prediction

ABSTRACT

Tornadoes are a co-occurring extreme that can be produced by landfalling tropical cyclones (TCs). These tornadoes can exacerbate the loss of life and property damage caused by the TC from which they were spawned. It is uncertain how the severe weather environments of landfalling TCs may change in a future climate and how this could impact tornado activity from TCs. In this study, we investigated four TCs that made landfall in the U.S. and produced large tornado outbreaks. We performed four-member ensembles of convective-allowing (4-km resolution) regional climate model simulations representing each TC in the historical climate and a mid-twenty-first century future climate. To identify potentially tornadic storms, or TC-tornado (TCT) surrogates, we used thresholds for three-hourly maximum updraft helicity and radar reflectivity, as tornadoes are not resolved in the model. We found that the ensemble-mean number of TCT-surrogates increased substantially (56–299%) in the future, supported by increases in most-unstable convective available potential energy, surface-to-700-hPa bulk wind shear, and 0–1-km storm-relative helicity in the tornado-producing region of the TCs. On the other hand, future changes in most-unstable convective inhibition had minimal influence on future TCT-surrogates. This provides robust evidence that tornado activity from TCs may increase in the future. Furthermore, TCT-surrogate frequency between 00Z and 09Z increased for three of the four cases, suggesting enhanced tornado activity at night, when people are asleep and more likely to miss warnings. All of these factors indicate that TC-tornadoes may become more frequent and a greater hazard in the future, compounding impacts from future increases in TC winds and precipitation.

1. Introduction

Tropical cyclones (TCs) are the deadliest and costliest natural disaster in the U.S., causing nearly 6,700 fatalities and $2.6 trillion in damages between 1980 and 2023 (NOAA Office for Coastal Management, 2023). Both human and financial costs from North Atlantic TCs continue to rise as coastal regions in the U.S. become more densely-populated over time. The population of coastal counties around the Gulf of Mexico grew by around 26% (3.0 million) between 2000 and 2017, while the coastal population over the Gulf of Mexico and North Atlantic combined grew by 16% (8.3 million), yielding around 60 million people who are vulnerable to TC impacts (Cohen 2019). Human and financial impacts from TCs will likely be exacerbated in the future; unmitigated climate change in a business-as-usual emissions scenario is projected to significantly enhance TC intensity and precipitation by the end of the 21st century, though with uncertainty in the magnitude of the enhancements (Patricola and Wehner 2018; Knutson et al., 2020; Carroll-Smith et al., 2021; Jung and Lackmann 2021). While TC intensity, precipitation, and storm surge are commonly studied, TC-tornadoes are an often-overlooked co-occurring extreme.

TC-tornadoes are a relatively common hazard produced by North Atlantic hurricanes, as 83% of hurricanes that made landfall along the Gulf of Mexico between 1950 and 2005 produced TC-tornadoes (Moore and Dixon 2011). TC-tornadoes have a history of impacting humans; 114 TC-tornadoes (6.5%) that occurred between 1995 and 2021 resulted in 403 injuries and 29 fatalities (Edwards 2010), while TC-tornadoes accounted for 10% of hurricane-related deaths in the U.S. between 1948 and 1972 (Novlan and Gray 1974) and 3% of North Atlantic TC-related deaths between 1963 and 2012 (Rappaport 2014). The majority of TC-tornadoes between 1995 and 2021 occurred during August

* Corresponding author.
E-mail addresses: dforbis@iastate.edu (D.C. Forbis), cmp28@iastate.edu (C.M. Patricola), ebercoshickey@lbl.gov (E. Bercos-Hickey), wgallus@iastate.edu (W.A. Gallus).

https://doi.org/10.1016/j.wace.2024.100684
Received 13 October 2023; Received in revised form 4 March 2024; Accepted 3 May 2024
Available online 4 May 2024

and September (70%) and between the daytime hours of 15Z and 00Z (60%) (Edwards 2010). TC-tornadoes can occur in multiple types of storm modes, primarily as discrete right-moving supercells and as supercells embedded within clusters, though non-supercellular TC-tornadoes can also occur (Edwards et al., 2012). TC-tornadoes may appear more subtle than their non-TC counterparts in Doppler radar data, given that TC-tornadoes are associated with an overall shallower mesocyclone, making the warning process for TC-tornadoes more difficult for meteorologists (Schneider and Sharp 2007; Spratt et al., 1997).

Environmental favorability for TC-tornado formation has multiple requirements, the most important being strong low-level vertical wind shear and strong storm-relative helicity (SRH) (Novlan and Gray 1974; Davies-Jones 1984). Helicity is important to the development of TC-tornadoes, as it enhances convection within the downshear region of mature TCs (Molinari and Vollaro 2008), with environmental helicity being particularly abundant in major TCs (Chen et al., 2021). Mid-level dry-air entrainment has also been associated with TCs that produced TC-tornado outbreaks (Curtis 2004) and is conducive to TC-tornado development (Hill et al., 1966; McCaul 1987, 1991) due to increased insolation-driven instability from dry air eroding a TC's cloudy regions (Curtis 2004), while enhanced lapse rates from dry air can also enhance instability (McCaul 1987; Hill et al., 1966). Dry-air entrainment may enhance evaporative cooling and therefore enhance lapse rates and instability (McCaul 1987; Baker et al., 2009), though this is location-dependent for dry air relative to a TC (Baker et al., 2009). Another important requirement is the presence of a high-moisture environment near the surface (Hill et al., 1966; McCaul 1987). The presence of low-level vertical wind shear (not to be confused with the deep-tropospheric wind shear that can inhibit TCs) is more important than buoyancy or convective available potential energy (CAPE) to TC-tornado development, allowing for TC-tornadoes to occur in low-CAPE environments (Novlan and Gray 1974). TCs that produce tornado outbreaks, however, tend to have relatively larger CAPE compared to TCs that have limited tornado activity (Baker et al., 2009).

The majority of TC-tornadoes occur within the eastern half of their TCs, as the kinematic environment is more favorable for TC-tornadoes in the downshear-right quadrant where deep-tropospheric wind shear increases (Moore et al., 2017; Schenkel et al., 2020; Edwards 2010). TC-tornadoes produced within the eastern half of TCs also tend to be wider and have longer path lengths than their counterparts within the western half of TCs (Moore et al., 2017). TC-tornadoes most commonly occur along coastlines, although the strongest TC-tornadoes tend to occur further inland and at higher latitudes (Moore et al., 2017). The risk for stronger TC-tornadoes increases further inland for highly-sheared TCs (Schenkel et al., 2021), resulting in a tradeoff between TC-tornado frequency and intensity the further inland a TC progresses. The increased frequency of TC-tornadoes along coastlines compared to inland areas may be attributed to a sharp, brief increase in supercell mesocyclone rotation prior to the host TC's landfall before supercell rotation gradually decreases throughout landfall (Baker et al., 2009). Given the tendency for stronger TC-tornadoes to occur further inland from where other TC impacts would occur, a larger population beyond those in coastal counties can be affected by TC-tornadoes.

Observed TC-tornado occurrence has increased since the mid-twentieth century. TC-tornadoes were observed in only 25% of hurricanes that impacted the U.S. between 1948 and 1972 (Novlan and Gray 1974), whereas 83% of hurricanes between 1950 and 2005 produced TC-tornadoes (Moore and Dixon 2011). While it is possible that environmental changes made TC-tornadoes more likely, the increase in observed TC-tornado occurrence may also be attributed to advancements in Doppler radar technology that improved meteorologists' ability to identify TC-tornadoes (Agee and Hendricks, 2011).

TC-tornadoes may become a more common hazard in the U.S. as climate change progresses. The number of tornado days during the autumn Atlantic hurricane season peak has increased over the southeastern U.S. from 1954–1983 to 1984–2013 (Agee et al., 2016). In addition, there has been a shift of tornado occurrence away from the Central Plains towards the southeast from 1959–1988 to 1989–2018 (Cao et al., 2021). Furthermore, a significant increase has occurred in both tornado reports over the southeastern U.S. since 1979 (Gensini and Brooks 2018) and the annual sum of daily maximum significant tornado parameter, which incorporates multiple factors such as SRH and CAPE to create an index for environmental favorability for strong tornadoes (Thompson et al., 2004). These factors, along with the tendency for most TC-tornadoes to occur from intense TCs (Hill et al., 1966; Novlan and Gray 1974; Moore and Dixon 2011), set a dangerous precedent for vulnerable regions throughout the U.S. as a warming climate may increase the frequency of stronger TCs (Bender et al., 2010).

Uncertainty remains regarding how climate change may affect TC-tornado occurrence, as there are few studies on the influence of climate change on TC-tornadoes. Previous studies on TC-tornadoes using convection-permitting regional model simulations produced mixed future projections. In particular, Carroll-Smith et al. (2021) investigated Hurricane Ivan (2004) using the pseudo-global warming method with future climate change perturbations from three general circulation models (GCMs). They found that the potential for future TC-tornadoes decreased in two of the experiments and increased in one of the experiments based on changes in updraft helicity, CAPE, and SRH.

Given that TC-tornadoes are a relatively overlooked hazard that have accounted for a substantial number of TC-related deaths in the U.S., there is considerable uncertainty as to how TC-tornado outbreaks will change in the future. The shift of tornado alley towards the southeastern U.S. where the population has been growing, along with an increase in tornadoes occurring outside of the typical severe weather season, emphasize the importance of this issue. Therefore, the objective of this study is to quantify future changes in TC-tornado activity and environmental favorability. We pose the following questions: how will TC-tornado activity change in the U.S. in a future climate, and how will the environmental favorability for TC-tornadoes change? To address these questions, we simulated historical TC events that produced large tornado outbreaks in both the historical climate and a possible future climate using a convection-permitting regional climate model. As far as we are aware, this study adds to one existing study on future TC-tornado projections (Carroll-Smith et al., 2021), and is novel in considering future changes in TC-tornadoes using multiple TC events.

2. Data and methods

2.1. Tropical cyclone cases

Four major hurricanes (Table 1) from the satellite era were selected for this study due to the large TC-tornado outbreaks they produced, including Hurricanes Ivan (2004), Katrina (2005), Rita (2005), and Harvey (2017). We attempted to include Hurricane Frances (2004) in the study. However, despite extensive testing, no initial condition and domain configuration could be found for which Frances would behave analogously in the future climate to its historical counterpart, therefore it was not possible to conduct meaningful analyses on Frances.

2.2. Data

Six-hourly TC track observations were obtained from the Atlantic

Table 1
Summary of Hurricanes selected for analysis.

Hurricane	First U.S. Landfall Date	Dissipation/Extratropical Transition Date	Number of Tornadoes Produced
Ivan	2004-09-16	2004-09-18	118
Katrina	2005-08-25	2005-08-31	59
Rita	2005-09-24	2005-09-26	97
Harvey	2017-08-26	2017-09-01	52

Hurricane Database (HURDAT2; Landsea and Franklin 2013) for comparison to simulated tracks. The observations include six-hourly TC position, landfall points, minimum sea-level pressure, and maximum sustained wind speed (Landsea and Franklin 2013). TC-tornado observations were obtained from the TCTOR dataset (Edwards 2010), which covers 1995–2021 and includes data for TC-tornado tracks, timeframe of occurrence, and casualties.

For initial and boundary conditions for the historical hindcasts (described in section 2.3) we used the European Centre for Medium-range Weather Forecasts ERA5 reanalysis (European Centre for Medium-Range Weather Forecasts, 2017; Hersbach et al., 2020). ERA5 consists of hourly 0.25° × 0.25° resolution atmospheric data at 38 vertical levels including the surface. In order to perturb the initial and boundary conditions for the future regional model simulations (described in section 2.3.1), we used future and historical climate data from the U.S. Department of Energy's Energy Exascale Earth System Model (E3SM) v1.1 (Bader et al. 2019, 2020), a participant in the Coupled Model Intercomparison Project 6 (CMIP6). The E3SM data we used are from 1° × 1° resolution coupled atmosphere-ocean simulations from the Historical experiment and the Shared Socioeconomic Pathways 5–8.5 (SSP5-8.5; Meinshausen et al., 2020) experiment. SSP5-8.5 assumes a business-as-usual/high greenhouse gas emissions scenario for the future. In addition, projected greenhouse gas concentrations in 2050 for the SSP5-8.5 scenario were based on Meinshausen et al. (2020) (Table 2), which we prescribed to the regional model simulations.

2.3. Convection-permitting climate model simulations

We performed convection-permitting regional climate model simulations using the Weather Research and Forecasting (WRF) model v4.3.0 (Skamarock et al., 2021) at a 4-km resolution with 50 vertical levels on the domains shown in Fig. 1a. The Mellor-Yamada-Janjić (MYJ) planetary boundary layer (PBL) scheme (Janjić 1994) and the Thompson cloud microphysics (MP) scheme (Thompson et al., 2008) were used, following Carroll-Smith et al. (2021). We used the Noah Land-Surface Model with four soil layers (Chen and Dudhia 2001). The Rapid Radiative Transfer Model (RRTMG) was used for shortwave and longwave radiation (Iacono et al., 2008). A four-member ensemble of simulations for each TC was produced using the stochastic kinetic energy backscatter scheme (SKEBS; Shutts 2005; Berner et al., 2011; Duda et al., 2016).

2.3.1. Future climate experiments

The future climate experiments represent how TCs may change by mid-century (2040–2060) under high greenhouse gas emissions. To achieve this, the initial conditions and surface and lateral boundary conditions for each TC were perturbed using the Pseudo-Global Warming (PGW) or "storyline" method (Schär et al., 1996; Patricola and Wehner 2018). We calculated the difference between the future climate (2040–2060) and the historical climate (1990–2009 for TCs that occurred in the 2000s, or 1995–2014 for TCs that occurred in the 2010s) and added the future climate perturbations to the initial and boundary conditions from the historical reanalysis. This was done in order to represent the TC in a warmer climate while retaining the synoptic conditions that produced the actual TC in the historical climate. Future climate change perturbations were calculated for the same month that the TC occurred and included spatial variations. The variables perturbed included relative humidity, surface pressure, sea-level pressure, air temperature, sea-surface temperature, surface temperature, and geopotential height. Vector winds were not perturbed to maintain TC steering flow conditions that were analogous to those in the historical climate, as TC tracks that are similar between the historical and future simulations better enable comparisons of TC characteristics. Soil moisture and temperature were not perturbed, as test simulations were relatively insensitive to changes in soil temperature, likely as it functions on larger timescales with respect to TCs, and since near-surface soils would become saturated quickly by the heavy TC rainfall. Greenhouse gas concentrations were prescribed from the SSP5-8.5 scenario for the year 2050 (Table 2).

We note that the future climate projections correspond to the climate sensitivity of the global model – here, E3SM – used to perturb WRF's initial and boundary conditions. It is possible that the future projections could correspond to a time earlier or later than mid-century, depending on when the prescribed level of warming is reached. Since previous studies (Carroll-Smith et al., 2021) have investigated the sensitivity of TC-tornado projections from multiple GCMs, we chose to prioritize producing simulations for multiple TC events rather than using multiple

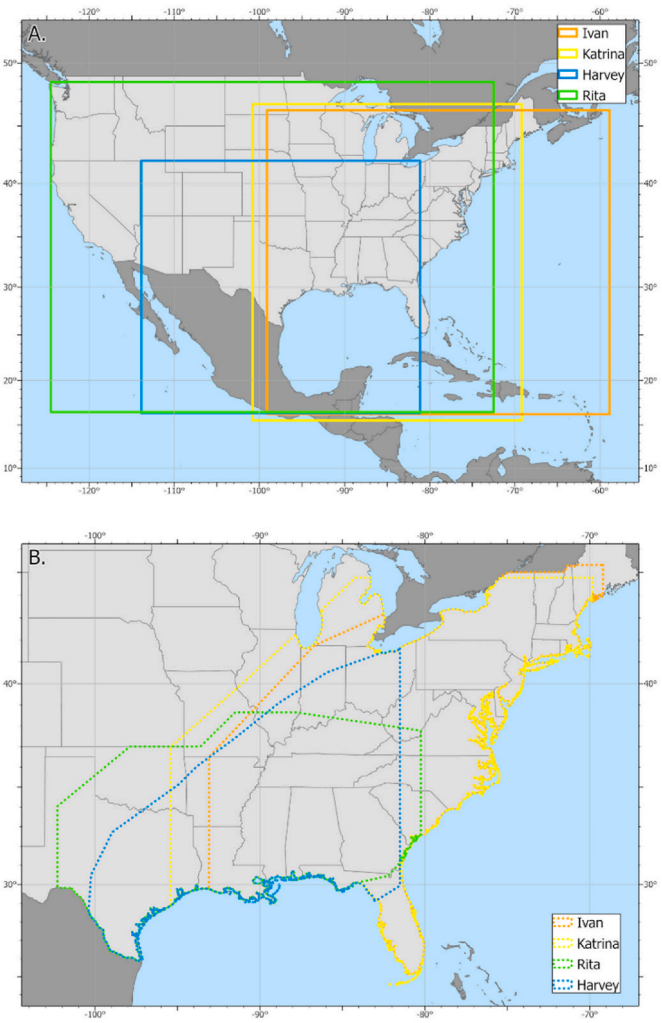

Fig. 1. (a) Domains used for 4-km simulations of each TC and (b) subdomains used for analyses.

Table 2
List of greenhouse gas species and their prescribed concentrations in the historical and future WRF simulations (Meinshausen et al., 2020; The University of Melbourne, 2020).

Greenhouse Gas Species	Historical	Future (SSP5-8.5 in 2050)
Carbon Dioxide (CO_2)	377.5 ppm (2004) 379.5 ppm (2005) 406.5 ppm (2017)	562.8 ppm
Methane (CH_4)	1,774.0 ppb	2,446.5 ppb
Nitrous Oxide (N_2O)	319.0 ppb	358.2 ppb
CFC-11 (CCl_3F)	251.0 ppt	138.0 ppt
CFC-12 (CCl_2F_2)	538.0 ppt	364.4 ppt
CFC-22 ($CHClF_2$)	169.0 ppt	49.9 ppt
Carbon Tetrachloride (CCl_4)	93.0 ppt	32.4 ppt

GCMs, in order to investigate a novel aspect of this problem.

2.3.2. TC Tracking

The simulated TC center was identified using the coordinates of the local minimum sea-level pressure every three hours. We also recorded the three-hourly maximum 10-m wind speeds associated with each TC.

2.3.3. TC-tornado surrogate identification

It was necessary to apply an algorithm to the WRF output to identify potentially-tornadic storms, or "TC-tornado (TCT) -surrogates," as individual tornadoes are not resolved in the model. We used a method adapted from Carroll-Smith et al. (2019, 2021) and Dawson et al. (2017). To summarize the method, simulated TCT-surrogates are identified based on model grid points that reach thresholds for maximum updraft helicity (UH) and simulated radar reflectivity. Observations are used for calibration to derive a UH threshold such that the percent of 4-km grid points identified as TCT-surrogates in the historical simulation would be equivalent to the observed tornado activity. The same thresholds are then used to identify TCT-surrogates in the future simulations. The details of the method are discussed below.

Maximum UH was calculated over three-hourly periods and between a layer 2–5 km above ground level (AGL), since this allowed for the TCT-surrogates to be identified without possible overrepresentation (Carroll-Smith et al., 2019, 2021). We ignored anticyclonic UH due to the rarity of anticyclonic tornadoes (Fujita 1977). Three-hourly maximum simulated radar reflectivity in 15-min intervals was used for radar reflectivity inputs.

We needed to determine UH thresholds to identify strong rotating updrafts. Each observed TC-tornado in the TCTOR dataset (Edwards 2010) includes the start and end points of the TC-tornado track, whereas the WRF output is on a 4-km grid. Therefore, the first step was to determine the approximate number of WRF grid points that would equivalently represent the observed TC-tornado activity. Note that the purpose is to calibrate to the aggregate statistics of observed TC-tornado activity. We emphasize that this method does not match UH tracks to observations and is not intended to hindcast the timing and location of observed TC-tornadoes, which would be unreasonable to expect a climate model to do. In order to translate the point-based observations into an equivalent on a 4-km grid, we generated 4-km buffers around the observed TC-tornado tracks and counted the number of points within the buffers to obtain a TCT-surrogate count representative of the calibrated observations (Table 3). We then calculated the percent of total subdomain grid points that were identified as TCT-surrogates, where the subdomain is the region in which TC-tornadoes were observed. Subtracting this percent from one yielded the percentile used to determine the UH threshold. We used two different methods to obtain UH thresholds in order to quantify uncertainty in the algorithm. For the first method, we calculated UH thresholds for each ensemble member, referred to as individualized thresholds. For the second method, all ensemble members were accounted for collectively to calculate the UH threshold, referred to as ensemble-wide thresholds. Finally, simulated TCT-surrogates were identified as points which met both the UH threshold and had a simulated radar reflectivity greater than 30 dBZ (Carroll-Smith et al., 2019, 2021). The same UH thresholds were used for the historical and future simulations.

UH thresholds obtained from calibration varied considerably between each TC, between 31 and 81 m^2/s^2, due to the differences between the number of observed TC-tornadoes for each TC and the number of potentially-tornadic storms produced by each simulation (Table 4). The methods use maxima of UH that are aggregated over time, therefore the number of TCT-surrogates counted in the historical hindcasts would be marginally greater than in the observed case due to spatial coincidence of grid points with high maximum UH at different times. We note that this method does not distinguish short-lived rotating supercells along the same track from long-lived supercells, thus the TCT-surrogate count represents overall TCT-surrogate occurrence (i.e., both frequency and longevity). In order to distinguish the two from each other, a method would be needed to group TCT-surrogate points into coherent tracks, which is beyond the scope of this study.

2.3.4. TC-quadrant analysis

Severe weather parameters, including maximum/most unstable CAPE (MUCAPE), maximum/most unstable convective inhibition (MUCIN), surface-to-700-hPa bulk wind shear (hereafter low-level BWS), and 0–1-km SRH, were analyzed for the northeastern TC quadrant where tornadic storms are most likely to occur. MUCAPE and MUCIN were analyzed for their roles in enhancing and suppressing convection, respectively (Trapp and Hoogewind 2016; Rasmussen et al., 2017). The surface-to-700-hPa layer was analyzed for BWS as low-level shear affects the height of developing mesocyclones that are associated with supercells (Markowski and Richardson 2014). We note that while low-level shear is important for TCTs, tropospheric shear (850–250 hPa) influences TCs themselves. SRH was analyzed over the 0–1-km AGL layer, as it is a more effective layer than 0–3 km AGL for identifying environments for potentially-tornadic supercells (Thompson et al., 2003; Rasmussen 2003), given that the lowest layers of SRH can enhance lifting mechanisms and low-level mesocyclones (Coffer and Parker 2017). For each three-hourly model output, we calculated the four environmental favorability parameters over quadrants relative to the TC center, including averages over the northeastern quadrant and the 95th-percentile values. Calculations were conducted within a 101-by-101-grid-point box, with the southwestern-most grid point coinciding with the TC center.

Table 4
Approximate maximum 3-hourly UH (m^2/s^2) thresholds for each of the four ensemble members and the ensemble-collective threshold for each Hurricane.

Hurricane	Ens. Member 1	Ens. Member 2	Ens. Member 3	Ens. Member 4	Ensemble-Collective
Ivan	35.1	47.1	49.2	40.2	43.0
Katrina	66.3	57.3	60.2	71.5	64.3
Rita	40.3	50.9	51.2	37.2	46.5
Harvey	71.3	78.7	65.9	81.1	74.1

Table 3
Simulation initializations and end dates, with dates for TCT-surrogate and environmental favorability analyses.

Hurricane	Initialization Date/ Time	End of Simulation	End of TCT-Surrogate and Severe Weather Analysis	Number of Tornadoes Analyzed	TCT-Surrogate Count Equivalent
Ivan (2004)	1800 UTC 2004-09-14	0000 UTC 2004-09-20	0900 UTC 2004-09-18	118	729
Katrina (2005)	0000 UTC 2005-08-28	0600 UTC 2005-08-31	0600 UTC 2005-08-31	57	275
Rita (2005)	1800 UTC 2005-09-22	0600 UTC 2005-09-26	0600 UTC 2005-09-26	97	455
Harvey (2017)	0000 UTC 2017-08-25	0000 UTC 2017-09-01	1500 UTC 2017-08-31	37	155

3. Results

3.1. TC tracks and intensity

We start by evaluating to what extent the model reproduces the observed TC tracks and landfall ahead of the TC-tornado outbreaks, as substantial deviations in the simulated relative to observed TC track can cause the TC to experience different environmental conditions and no longer be comparable to the observed TC. The historical hindcasts for each TC represented the observed TC tracks reasonably well, as there are only relatively minor deviations from the observed track for each ensemble member and the ensemble mean before landfall and during the time when the observed TC-tornado outbreaks occurred (Fig. 2). Furthermore, future changes in simulated TC tracks relative to the

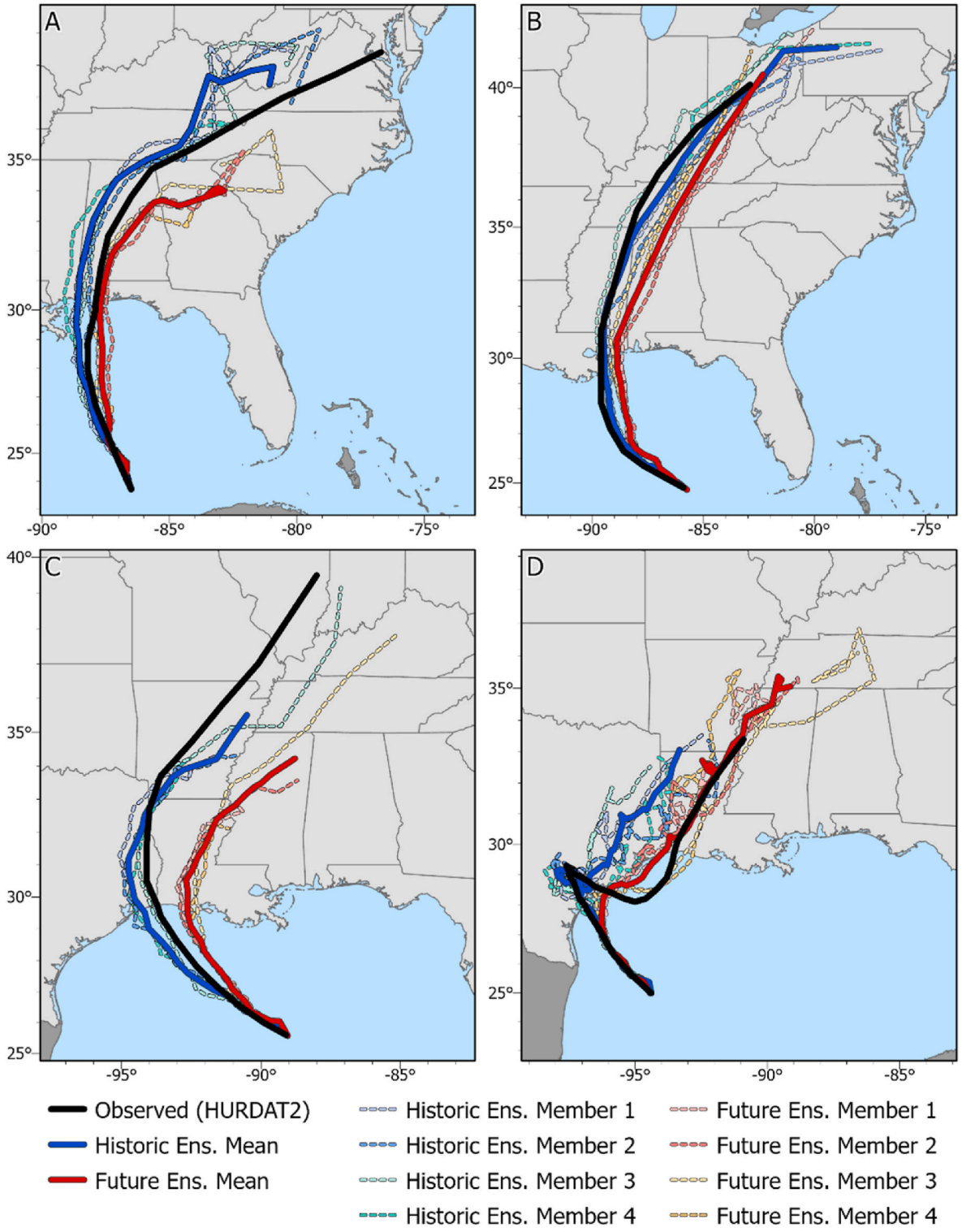

Fig. 2. Observed TC tracks from HURDAT2 (black), with simulated TC tracks from individual ensemble members (dashed) and the ensemble-mean (solid) from the historical (blue) and future (red) experiments for Hurricanes (a) Ivan, (b), Katrina, (c) Rita, and (d) Harvey. Both the observed and simulated tracks are shown only for the duration of the simulation. (For interpretation of the references to colour in this figure legend, the reader is referred to the Web version of this article.)

historical are relatively minor for all TCs, allowing comparison between the historical and future simulations. The landfall points of the historical ensemble-mean for the four TCs matched closely with observed, with deviations ranging from nearly zero km for Harvey to 77 km for Ivan (Fig. 2).

All TCs in the historical ensemble strengthened into hurricanes (10-m wind of at least 64 kts) after model spin-up but were weaker compared to observed maximum 10-m wind speeds (Fig. 3) and minimum sea-level pressure (figure not shown). This may be due to the model's 4-km resolution (Davis 2018) and the parameterizations used, as different combinations of PBL and microphysics parameterizations can influence the potential maximum intensity of simulated TCs relative to observations (Davis and Bosart 2002; Li and Pu 2008; Nolan et al., 2021). All ensemble members for all TCs projected a future increase in TC intensity, which was consistent with the typical climate change response in other studies. The ensemble-mean peak 10-m wind speeds increased by 10–20 kts for the four TCs (Fig. 3), while minimum sea-level pressure decreased by 16–30 hPa (figure not shown).

3.2. TCT-surrogates

The historical simulations produced TCT-surrogates in the general regions where observed TC-tornadoes occurred for all four TCs (Fig. 4), further demonstrating that the hindcasts were suitable for addressing our research question. We note that we do not expect the model to reproduce the exact locations of each of the observed TCTs, just as it is unrealistic to forecast the exact locations of TCTs days ahead of time. We note that the historical simulations show a bias for TCT-surrogate occurrence in the landfall region, even when observed TCTs for the corresponding TC(s) were more evenly distributed in space or primarily over inland regions. Note that the TCT-surrogate activity in the historical simulations has the appearance of being greater than observed because it consists of 4-member ensembles.

As each ensemble member for each TC used different UH thresholds to identify TCT-surrogates, we evaluated how sensitive the ensemble-mean TCT-surrogate counts were to using two methods for determining UH thresholds, namely individualized UH thresholds for each ensemble member and an ensemble-wide UH threshold. Overall

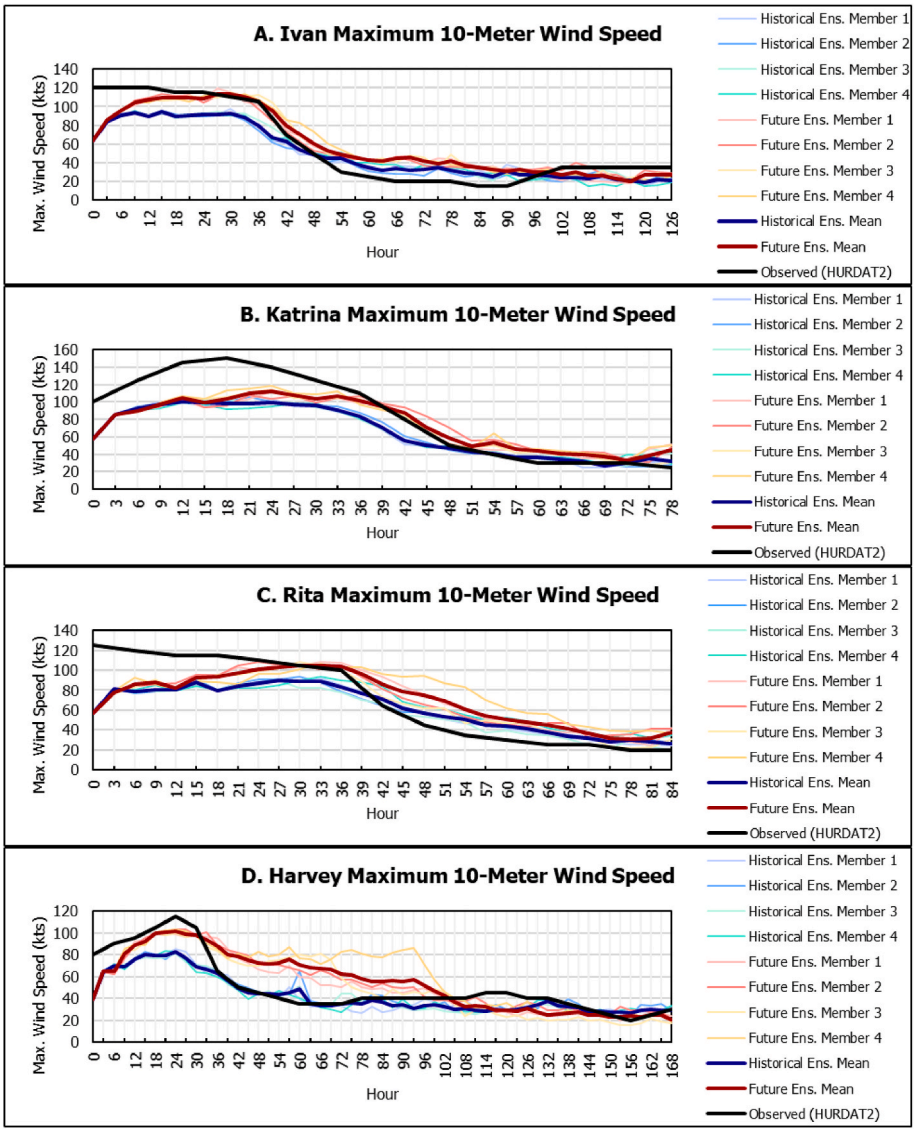

Fig. 3. Maximum 10-m wind speed (kts) from observations (black), historical ensemble members (thin blue/cyan lines) and ensemble-mean (thick dark-blue line), and future ensemble members (thin red/yellow lines) and ensemble-mean (thick dark-red line) for Hurricanes (a) Ivan (b), Katrina (c), Rita, and (d) Harvey. The x-axis represents hours since model initialization. (For interpretation of the references to colour in this figure legend, the reader is referred to the Web version of this article.)

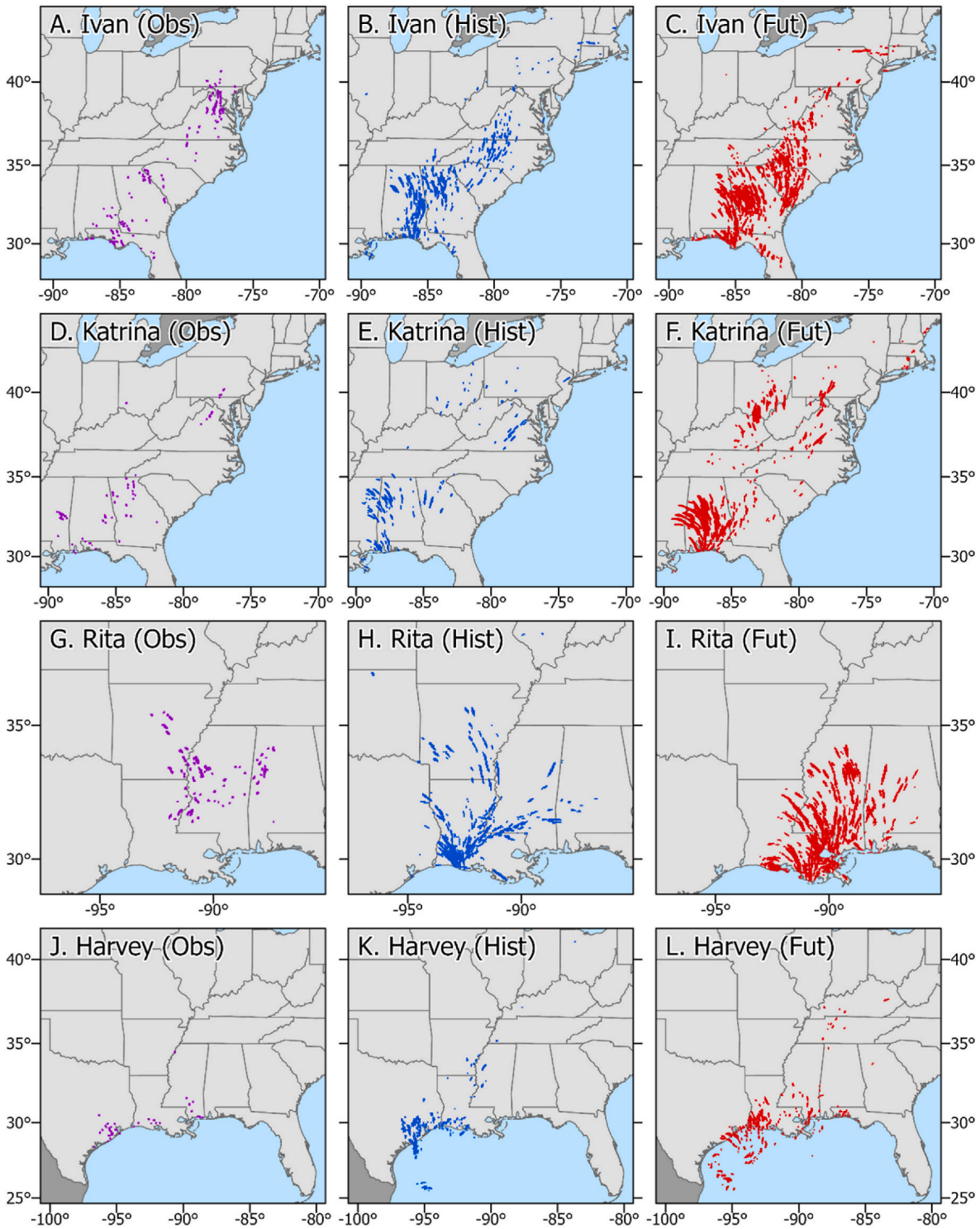

Fig. 4. Observed TC-tornadoes and simulated TCT-surrogates (using individualized UH thresholds for ensembles) for Hurricanes Ivan, Katrina, Rita, and Harvey, respectively, from (a, d, g, and j) observations and the (b, e, h, k) historical and (c, f, i, l) future simulations. Simulated TCT-surrogates for Harvey are included over ocean. Simulated TCT-surrogates are shown for the 4-member ensemble.

ensemble-mean TCT-surrogate counts had minimal sensitivity to the method in both climates, with no changes in the overall climate change response in TCT-surrogates (Fig. 5). TCT-surrogate counts in the historical simulations when using individualized UH thresholds for each ensemble member were slightly greater than the observed TCT-surrogate count used for calibration; increases in TCT-surrogate counts for the historical simulations, relative to observations used for calibration, ranged from 3% for Ivan to up to 8% for Rita for the three TCs that included land-based TCT-surrogates. There was a 48% increase in historical TCT-surrogates for Harvey relative to observations because we included simulated TCT-surrogates over the Gulf of Mexico, for which observations were unavailable, for reasons explained below. Using an ensemble-wide threshold for UH resulted in an 8% increase in historical TCT-surrogates for Ivan, relative to observations, while the number of TCT-surrogates for Rita and Harvey increased by a smaller amount relative to using individualized UH thresholds. The number of TCT-

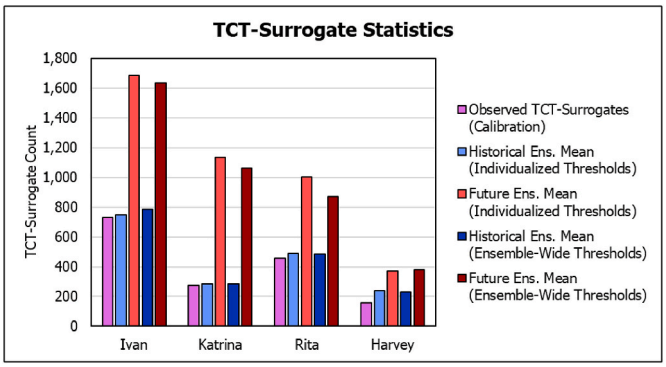

Fig. 5. Observed TCT-surrogate counts (for calibration) and ensemble-mean historical and future TCT-surrogate counts derived using both methods for UH thresholds for each TC.

surrogates remained constant for Katrina, regardless of the method used.

Geographic distributions of TCT-surrogates were generally similar between the historical and future ensembles (Fig. 4), with some relatively minor regional shifts associated with shifts in TC landfall. Nonetheless, our results are valid given that the simulated TC landfalls were close to observed, while the TC tracks further inland remained analogous despite changes in translation speed, (particularly in the future for Ivan, Rita, and Harvey). This enabled us to compare between the two climates without adjustment to the TCT-surrogate identification method, which is primarily land-based. On the other hand, a shift occurred in Harvey's track between the historical and future simulations that impacted the time Harvey spent over land. Therefore, we included TCT-surrogates that occurred over the Gulf of Mexico in the TCT-surrogate counts for Harvey. Had we not included the ocean-based TCT-surrogates for Harvey, the future TCT-surrogate projections would have been substantially impacted by the future shift in Harvey's track, given the difference in time Harvey spent over land during the two experiments.

This exception for Harvey relies on the assumption that there is not a systematic difference in the future projection of TCT-surrogates depending on whether the TCT-surrogates are considered only over land or over both land and ocean. We tested this assumption with Katrina, as Katrina's track, landfall location, and regional TCT-surrogate occurrence were relatively similar between the historical and future simulations. We found no substantial differences between the future projections of TCT-surrogates occurring over land only (increase of 299%) compared to both ocean and land together (increase of 282%) (Fig. 6). This provided justification for including TCT-surrogates over ocean for Harvey's analysis, for which several TCT-surrogates were identified over the Gulf of Mexico near the coastline in the future simulation.

We then quantified the future change in ensemble-mean TCT-surrogate counts and notably found a robust increase in the future climate for all four TCs (Fig. 5). Ensemble-mean TCT-surrogate counts in the future ensemble (using an individualized threshold) were the greatest for Ivan (1,686), while the greatest relative change from the historical simulations to the future experiments occurred for Katrina (+299%). The relative increase in TCT-surrogate counts for Ivan (+125%) and Rita (+105%) were similar in magnitude, while Harvey had the smallest increase in TCT-surrogate counts (+56%). Similar relative increases were projected for all TCs in the future when using an ensemble-wide UH threshold, ranging from 66% for Harvey to 273% for Katrina, with increases of 109% and 80% for Ivan and Rita, respectively.

In addition to changes in the number and spatial distributions of TCT-surrogates between the historical and future simulations, the temporal characteristics of TCT-surrogate occurrence also changed (Fig. 7). We investigated the diurnal timing of the TCT-surrogates since tornadoes that occur at night are more dangerous because they are hard to see and it is more likely that people may miss warnings when they are asleep. The relative occurrence of evening and nighttime TCT-surrogates between 00Z–09Z (7PM–4AM Central Daylight Savings Time (CDT)) increased from the historical into the future for three of the four TCs (Ivan, Katrina, and Rita). Considering the three aforementioned TCs, the percentage of TCT-surrogates that occurred between 00Z–09Z increased from 11–23% in the historical to 23–35% in the future. However, Harvey's nocturnal TCT-surrogate occurrence decreased from 47% in the historical to 34% in the future. Despite these increases in nocturnal TCT-surrogates, the majority of TCT-surrogate counts occurred between 18Z–00Z for Ivan and Katrina, and a large portion occurred during those hours for Rita and Harvey.

We found that the diurnal changes in TCT-surrogates were supported by a combination of environmental conditions including future increases in or maintenance of nocturnal MUCAPE, low-level BWS, and 0–1-km SRH for Ivan, Katrina, and Rita, whereas future environmental changes limited the increase of Harvey's nocturnal TCT-surrogates (Fig. 8). Nocturnal ensemble-mean MUCAPE, averaged for each 00Z, 03Z, 06Z, and 09Z twice during a 48-hour period starting approximately six hours before landfall, increased by 319–600 J/kg (42–134%) for all four TCs. Nocturnal low-level BWS strengthened by 2–8 kts (6–19%), and 0–1-km SRH was enhanced by 94–173 m^2/s^2 (16–36%). Despite having the largest relative increase in nocturnal SRH and the highest nocturnal MCAPE, nocturnal TCT-surrogate count increases for Harvey were likely hindered by the overall small magnitude of Harvey's 0–1-km SRH, as it was considerably smaller than for the other TCs, regardless of climate. These diurnal responses occurred despite a general trend for future TC landfall to occur later (usually during the daytime) than in the historical simulation (Tables 5 and 6) due to a combination of generally slower translation speeds and shifts in landfall location associated with shifts in TC tracks (with the latter particularly true for Harvey).

3.3. *Environmental favorability within the northeastern TC quadrant*

We analyzed the severe weather environment in which the TCT-surrogates occurred, focusing on the northeastern TC quadrant, to quantify changes in favorability for TC-tornadoes between the historical and future climates. Measures for the instability (MUCAPE) and capping (MUCIN) of the atmosphere, low-level wind shear, and storm-relative helicity were used, as they are important in the development of potentially-tornadic storms, with low-level wind shear being more important than MUCAPE for TC-tornadoes (Novlan and Gray 1974).

Ensemble-mean quadrant-averaged MUCAPE in the northeastern TC quadrant increased robustly in the future for Ivan, Katrina, and Rita (Fig. 9a), partly due to warmer ocean waters; MUCAPE increased by 677–975 J/kg (65–89%) for the three TCs, while Harvey's MUCAPE only increased by 195 J/kg or 17%. As a result of the future increase in instability, quadrant-averaged MUCAPE ranged between 1,373–2,068 J/kg for the future simulations of the four TCs. Like the quadrant-average, changes in 95th-percentile values of MUCAPE, which were used to represent extreme MUCAPE in the northeastern quadrant of each TC, also increased by 1,208–1,519 J/kg (71–81%) for the three aforementioned TCs and by 214 J/kg (8%) for Harvey. This increase resulted in 95th-percentile MUCAPE ranging between 2,783–3,403 J/kg for TCs in the future climate.

Ensemble-mean quadrant-averaged MUCIN (for which positive MUCIN indicates decreased environmental favorability), changed little for the four TCs (Fig. 9b), with future increases of approximately 2 J/kg and 6 J/kg for Katrina and Rita, respectively, a decrease of 2 J/kg for Harvey, and approximately no change for Ivan. These changes in quadrant-averaged MUCIN, or lack thereof, resulted in future MUCIN ranging approximately between 7–17 J/kg. 95th-percentile values of MUCIN changed similarly, with an increase of 3–31 J/kg for three of the TCs, whereas MUCIN decreased by 9 J/kg for Harvey. These changes resulted in future extreme MUCIN that ranged between 34–76 J/kg.

Future increases in low-level BWS were similar for all four TCs, with

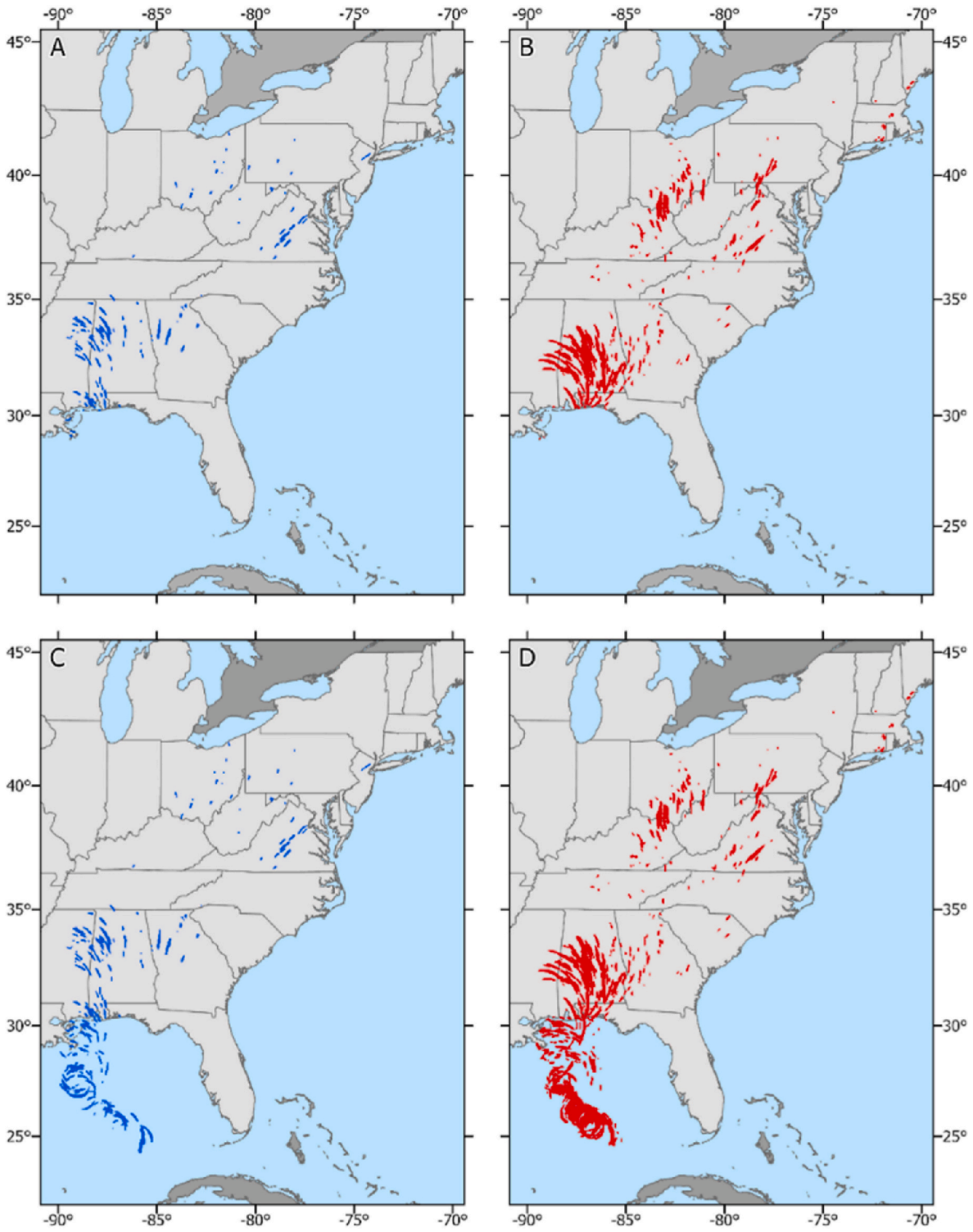

Fig. 6. TCT-surrogates (using individualized UH thresholds) for all ensemble members for Hurricane Katrina excluding ocean in the (a) historical and (b) future simulations and including ocean in the (c) historical and (d) future simulations.

quadrant-averaged ensemble-mean BWS increases of 3–5 kts (7–16%), resulting in future quadrant-averaged BWS of 29–47 kts (Fig. 9c). The 95th-percentile values of BWS increased by 5–9 kts (9–15%) for the four TCs. This resulted in TCs in the future climate having extreme values of BWS of 48–75 kts. As with BWS, quadrant-averaged ensemble-mean 0–1-km SRH increased for all four TCs (Fig. 9d). Future ensemble-mean quadrant-averaged SRH ranged between 346–653 m^2/s^2, representing an increase of 74–129 m^2/s^2 (14–59%) relative to the historical. 95th-percentile values of 0–1-km SRH ranged between 701–1,481 m^2/s^2 in the future, representing an increase of 173–301 m^2/s^2 (15–34%). The future increases in BWS and SRH are likely associated with the increase in 10-m winds from the TCs.

4. Discussion and conclusions

The purpose of this study was to investigate how TC-tornado activity

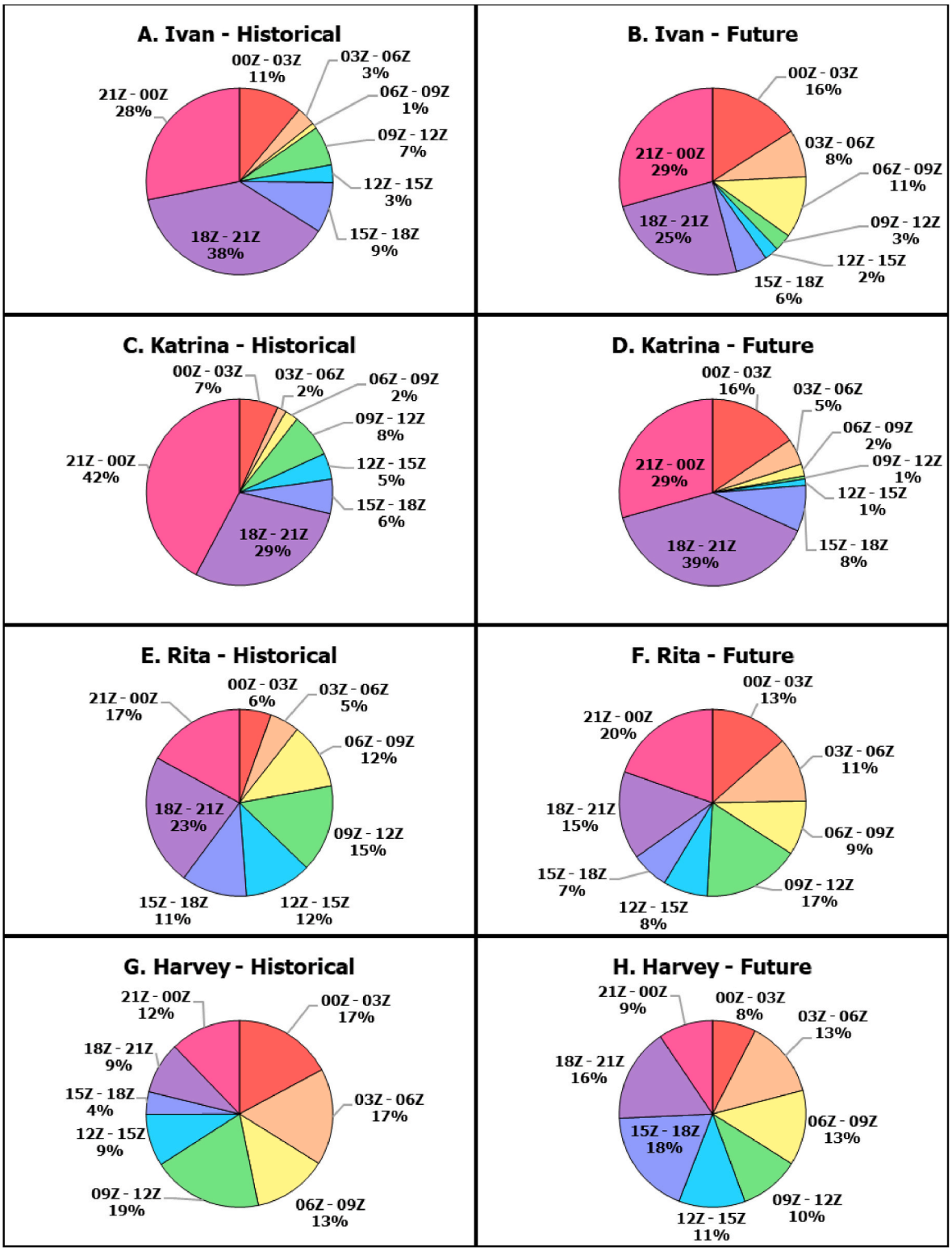

Fig. 7. Three-hourly distribution (using individualized UH thresholds) of simulated TCT-surrogate occurrence throughout the analysis period from the four-member ensembles for Hurricanes Ivan, Katrina, Rita, and Harvey, respectively, from the (a, c, e, and g) historical and (b, d, f, and h) future simulations.

and environmental favorability may change in the U.S. in the future. We investigated four historically-impactful Hurricanes (Ivan, Katrina, Rita, and Harvey) that produced substantial TC-tornado outbreaks using ensembles of convection-permitting regional model (WRF) simulations. The simulations represented the TCs in the historical climate in which they actually occurred and the TCs if similar events were to occur in a future warmer climate (mid-twenty-first century under a high emissions scenario, based on E3SM), using the pseudo-global warming method. We found that the future number of TCT-surrogates, which represent potentially-tornadic thunderstorms in TCs, increased by up to a factor of four times the historical counts (56–299%). This increase was robust across all four TCs considered. The projected increases in TCT-

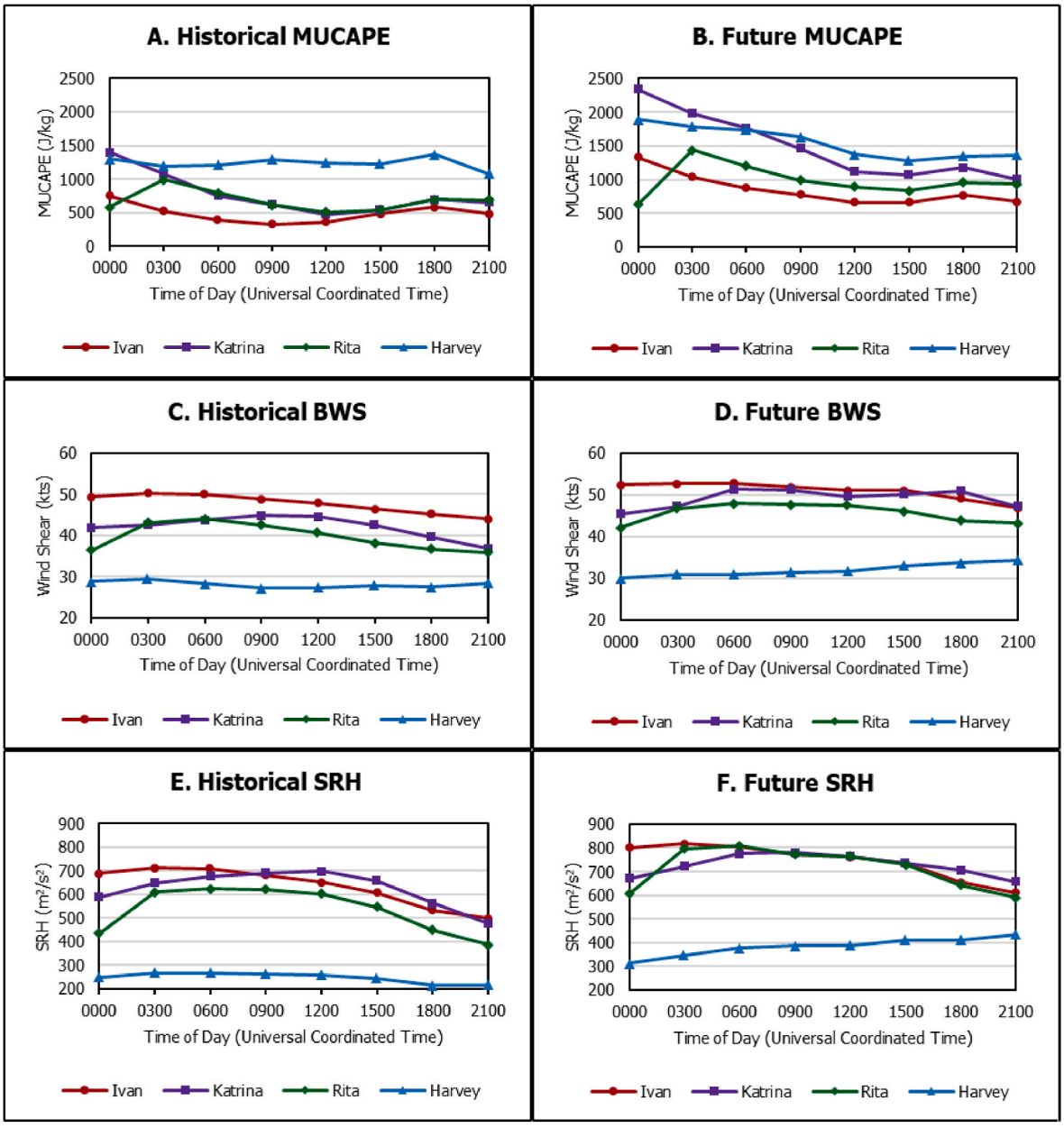

Fig. 8. Diurnal changes in quadrant-averaged ensemble-mean MUCAPE (J/kg) from the (a) historical and (b) future simulations, low-level BWS (kts) from the (c) historical and (d) future simulations, and 0–1-km SRH (m^2/s^2) from the (e) historical and (f) future simulations. Values were considered over a 48-hour period, starting six hours before the ensemble-mean landfall time (rounded to the nearest third hour) for each TC's historical ensemble. Each value represents the average of two times during the 48-hour period (e.g., 00z during the first 24 hours and 00z during the second 24 hours).

Table 5
Approximate simulated first landfall times (Universal Coordinated Time) for each ensemble member's TC from the historical simulations. Yellow shading represents daytime landfalls (from sunrise to sunset), whereas blue shading represents nighttime landfalls (from sunset to sunrise, NOAA Global Monitoring Laboratory/Earth System Research Laboratories, 2022).

TC Name	Ens. Member 1	Ens. Member 2	Ens. Member 3	Ens. Member 4
Ivan	9/16/2004 6:17	9/16/2004 5:06	9/16/2004 9:20	9/16/2004 7:17
Katrina	8/29/2005 6:59	8/29/2005 8:15	8/29/2005 7:24	8/29/2005 6:47
Rita	9/24/2005 9:10	9/24/2005 8:29	9/24/2005 7:02	9/24/2005 14:11
Harvey	8/26/2017 5:28	8/26/2017 5:02	8/26/2017 4:25	8/26/2017 3:27

Table 6
Same as Table 5, but from the future simulations.

TC Name	Ens. Member 1	Ens. Member 2	Ens. Member 3	Ens. Member 4
Ivan	9/16/2004 9:01	9/16/2004 7:18	9/16/2004 9:39	9/16/2004 11:24
Katrina	8/29/2005 14:57	8/29/2005 15:00	8/29/2005 15:10	8/29/2005 16:06
Rita	9/24/2005 11:02	9/24/2005 8:59	9/24/2005 6:44	9/24/2005 15:54
Harvey	8/26/2017 15:16	8/27/2017 13:01	8/27/2017 20:21	8/26/2017 10:03

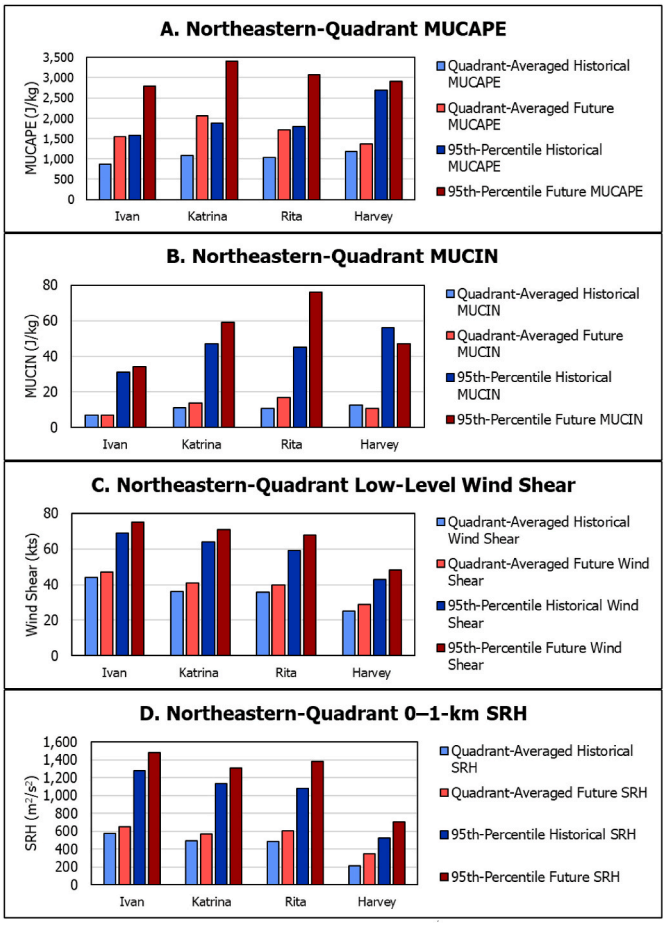

Fig. 9. Northeastern-quadrant statistics (average and 95th percentile) during the analysis period of each TC for: (a) MUCAPE (J/kg), (b) MUCIN (J/kg), (c) low-level BWS (kts), (d) 0–1-km SRH (m^2/s^2) from the historical and future ensemble-averages.

surrogates suggest that tornadic storms occurring in future landfalling major hurricanes may increase in frequency and/or longevity.

The future increases in TCT-surrogates are supported by a more favorable environment for severe storms. We found substantial future increases in MUCAPE, low-level BWS, and 0–1-km SRH in the northeastern quadrant of the TCs, with average MUCAPE increasing by 17–89%, average BWS by 7–16%, and average 0–1-km SRH by 14–59%. Enhancement of MUCAPE suggests that future TC-tornado outbreaks may become more likely (Baker et al., 2009). Enhancements in BWS and 0–1-km SRH should enhance vertical vorticity and streamwise vorticity, respectively, for potentially-tornadic supercells embedded in TCs, enhancing their probabilities of occurrence in addition to the highly-buoyant environment. Future increases in MUCIN in three of the four TCs played little role in the future TCT-surrogate increases.

Our results are in agreement with Carroll-Smith et al. (2021)'s PGW simulation that was perturbed by the Model for Interdisciplinary Research on Climate (MIROC) version 5. They found an increase in future TCT-surrogates for Hurricane Ivan. Enhancements in average SRH and BWS during landfall were the greatest for the experiment perturbed by MIROC, while CAPE was also substantially enhanced (Carroll-Smith et al., 2021), consistent with our findings. Our results differ from PGW simulations perturbed using the Community Climate System Model (CESM) version 4 and Geophysical Fluid Dynamics Laboratory Climate Model (GFDL) version 3, which projected a future decrease in TCT-surrogates (Carroll-Smith et al., 2021). This may be due to the climate sensitivity to greenhouse gas forcing in E3SM, as average sea-surface temperatures in the Gulf of Mexico increased by approximately 2.6 °C and 2.7 °C in August and September, respectively, for simulations of TCs that occurred during the 2000s.

Notably, the diurnal timing of TCT-surrogates shifted considerably for three of the four TCs, with increased relative occurrence at nighttime (00Z–09Z). This may be due to multiple factors, including enhanced buoyancy in the future climate increasing the longevity of potentially-tornadic storms embedded within a TC and overcoming any enhancement of CIN; having sufficient nocturnal CAPE for prolonged convection; and enhanced BWS and SRH providing the necessary shear for rotating supercells. This enhancement of nocturnal TCT-surrogates is consistent with the late-twenty-first-century results for nocturnal tornadic storms in Bercos-Hickey et al. (2021), which showed high SRH and CAPE in the nocturnal environment's simulation combined with low CIN, resulting in greater storm activity. Though CIN increased slightly in our simulations where TC-tornado activity was greatest, the overall environmental conditions supported an increase in TCT-surrogates as sufficient forcing within the TC environment was present, increasing the severity of the convection (Rasmussen et al., 2017).

As the analyses of Carroll-Smith et al. (2021) were carried out at 3-km resolution, we are uncertain on how updraft helicity and their TCT-surrogate identification thresholds would scale to a 4-km grid. To account for this uncertainty, we used two methods to quantify a maximum updraft helicity threshold, though some of the updraft helicity thresholds used may be lower than required for TC-tornadoes. In addition, updraft helicity thresholds for TC-tornadoes may or may not be similar to updraft helicities for non-TC-tornadic storms due to differences in updrafts and the environment between TC-tornadic storms and non-TC-tornadic storms. There is also uncertainty due to the fact that the model does not directly resolve tornadoes, thus it is uncertain which storms would have actually produced tornadoes. The strong warming perturbation from E3SM also introduces uncertainty, primarily with respect to when such an environment may be realized during the 21st century, as such an environment may occur later or earlier than 2040–2060.

In summary, TC-tornado outbreaks from major hurricanes in the mid-21st century may be enhanced by climate change, with a more favorable environment for TC-tornadogenesis in the region of TCs where TC-tornadoes are most likely to occur. Our results indicate that future TC-tornado outbreaks may become more dangerous, not only because of an increase in frequency and/or duration of TC-tornadoes, but also because of enhanced TC-tornado outbreaks at night for three of the four TCs. This would compound an already difficult warning process, as

people may be more likely to miss tornado warnings at night when they are asleep. Future work should be conducted to narrow the range of uncertainty on how much TC-tornado activity may increase in a changing climate, including experiments using other GCMs for climate change perturbations. As our results pertain to major hurricanes that are capable of producing TC-tornado outbreaks, additional research would be helpful to investigate weaker TCs that produced TC-tornadoes, as well as TCs that produced low numbers of TC-tornadoes, regardless of intensity, to determine if future analogs of TCs that produced few TC-tornadoes would be capable of producing stronger outbreaks in the future.

CRediT authorship contribution statement

Dakota C. Forbis: Conceptualization, Data curation, Formal analysis, Investigation, Methodology, Software, Validation, Visualization, Writing – original draft. **Christina M. Patricola:** Conceptualization, Funding acquisition, Methodology, Project administration, Resources, Software, Supervision, Writing – original draft, Writing – review & editing. **Emily Bercos-Hickey:** Software, Writing – review & editing. **William A. Gallus:** Writing – review & editing.

Declaration of competing interest

The authors declare the following financial interests/personal relationships which may be considered as potential competing interests:

Dakota C. Forbis reports financial support, article publishing charges, equipment, drugs, or supplies, and travel were provided by Iowa State University. If there are other authors, they declare that they have no known competing financial interests or personal relationships that could have appeared to influence the work reported in this paper.

Data availability

Data will be made available on request.

Acknowledgements

This research was supported by the US Department of Energy, Office of Science, Office of Biological and Environmental Research, Earth and Environmental Systems Modeling Program, under Early Career Research Program Award Number DE-SC0021109. This work used the Extreme Science and Engineering Discovery Environment (XSEDE) computing resource Stampede2 and Ranch, which is supported by National Science Foundation grant number ACI-1548562, through allocations ATM190012, ATM190016, and EES230023. The authors acknowledge the Texas Advanced Computing Center (TACC) at The University of Texas at Austin for providing HPC resources that have contributed to the research results reported within this paper. URL: http://www.tacc.utexas.edu. The data were provided by the Research Data Archive (RDA) of the Computational and Information Systems Laboratory at the National Center for Atmospheric Research. NCAR is supported by grants from the National Science Foundation. Data were obtained from the Energy Exascale Earth System Model project, sponsored by the U.S. Department of Energy, Office of Science, Office of Biological and Environmental Research. This research was supported as part of the Energy Exascale Earth System Model (E3SM) project, funded by the U.S. Department of Energy, Office of Science, Office of Biological and Environmental Research. The authors thank one anonymous reviewer for their constructive comments that helped improve the manuscript.

References

Agee, E.M., Hendricks, A., 2011. An Assessment of the Climatology of Florida hurricane-Induced tornadoes (HITs): technology versus Meteorology. J. Clim. 24, 5218–5222. https://doi.org/10.1175/JCLI-D-11-00235.1.

Agee, E., Larson, J., Childs, S., Marmo, A., 2016. Spatial Redistribution of U.S. Tornado activity between 1954 and 2013. J. Appl. Meteor. Climatol. 55, 1681–1697. https://doi.org/10.1175/JAMC-D-15-0342.1.

Bader, David C., Leung, Ruby, Taylor, Mark, McCoy, Renata B., 2019. E3SM-Project E3SM1.1 model output prepared for CMIP6 CMIP historical. Version 20220407. Earth System Grid Federation. https://doi.org/10.22033/ESGF/CMIP6.11485.

Bader, David C., Leung, Ruby, Taylor, Mark, McCoy, Renata B., 2020. E3SM-Project E3SM1.1 model output prepared for CMIP6 ScenarioMIP ssp585. Version 20220407. Earth System Grid Federation. https://doi.org/10.22033/ESGF/CMIP6.15179.

Baker, A.K., Parker, M.D., Eastin, M.D., 2009. Environmental Ingredients for supercells and tornadoes within hurricane Ivan. Weather Forecast. 24, 223–243. https://doi.org/10.1175/2008WAF2222146.1.

Bercos-Hickey, E., Patricola, C.M., Gallus Jr., W.A., 2021. Anthropogenic influences on tornadic storms. J. Climate 34, 8989–9006. https://doi.org/10.1175/JCLI-D-20-0901.1.

Bender, M.A., Knutson, T.R., Tuleya, R.E., Sirutis, J.J., Vecchi, G.A., Garner, S.T., Held, I. M., 2010. Modeled impact of Anthropogenic warming on the frequency of intense Atlantic hurricanes. Science 327, 454–458. https://doi.org/10.1126/science.1180568.

Berner, J., Ha, S.-Y., Hacker, J.P., Fournier, A., Snyder, C., 2011. Model uncertainty in a Mesoscale ensemble prediction system: stochastic versus multiphysics representations. Mon. Wea. Rev. 139, 1972–1995. https://doi.org/10.1175/2010MWR3595.1.

Cao, Z., Cai, H., Zhang, G.J., 2021. Geographic shift and environment change of U.S. Tornado activities in a warming climate. Atmosphere 12, 567. https://doi.org/10.3390/atmos12050567.

Carroll-Smith, D.L., Dawson, L.C., Trapp, R.J., 2019. High-resolution real-data WRF modeling and verification of tropical cyclone tornadoes associated with hurricane ivan (2004). Electronic J. of Severe Storms Meteor 14, 1–37. https://ejssm.org/archives/2019/vol-14-2-2019/.

Carroll-Smith, D., Trapp, R.J., Done, J.M., 2021. Exploring inland tropical cyclone rainfall and tornadoes under future climate conditions through a case study of hurricane ivan. J. Appl. Meteor. Climatol. 60, 103–118. https://doi.org/10.1175/JAMC-D-20-0090.1.

Chen, F., Dudhia, J., 2001. Coupling an advanced land surface-hydrology model with the Penn State–NCARMM5 modeling system. Part I: model implementation and sensitivity. Mon. Wea. Rev. 129, 569–585. https://doi.org/10.1175/1520-0493(2001)129,0569:CAALSH.2.0.CO;2.

Chen, N., Tang, J., Zhang, J.A., Ma, L.-M., Yu, H., 2021. On the distribution of helicity in the tropical cyclone boundary layer from dropsonde composites. Atmos. Res. 249, 1–11. https://doi.org/10.1016/j.atmosres.2020.105298.

Coffer, B.E., Parker, M.D., 2017. Simulated supercells in nontornadic and tornadic VORTEX2 environments. Mon. Wea. Rev. 145, 149–180. https://doi.org/10.1175/MWR-D-16-0226.1.

Cohen, D., 2019. About 60. 2M Live in Areas Most Vulnerable to Hurricanes. United States Census Bureau. https://www.census.gov/library/stories/2019/07/millions-of-americans-live-coastline-regions.html. (Accessed 2 December 2022).

Curtis, L., 2004. Midlevel dry intrusions as a factor in tornado outbreaks associated with landfalling tropical cyclones from the atlantic and Gulf of Mexico. Wea. Forecasting 19, 411–427. https://doi.org/10.1175/1520-0434(2004)019<0411:MDIAAF>2.0.CO;2.

Davies-Jones, R., 1984. Streamwise vorticity: the origin of updraft rotation in supercell storms. J. Atmos. Sci. 41, 2991–3006. https://doi.org/10.1175/1520-0469(1984)041<2991:SVTOOU>2.0.CO;2.

Davis, C., Bosart, L.F., 2002. Numerical simulations of the genesis of hurricane diana (1984). Part II: sensitivity of track and intensity prediction. Mon. Weather Rev. 130, 1100–1124. https://doi.org/10.1175/1520-0493(2002)130<1100:NSOTGO>2.0.CO;2.

Davis, C.A., 2018. Resolving tropical cyclone intensity in models. Geophys. Res. Lett. 45, 2082–2087. https://doi.org/10.1002/2017gl076966.

Dawson, L.C., Romine, G.S., Trapp, R.J., Baldwin, M.E., 2017. Verifying supercellular rotation in a convection-permitting ensemble forecasting system with radar-derived rotation track data. Wea. Forecasting 32, 781–795. https://doi.org/10.1175/WAF-D-16-0121.1.

Duda, J.D., Wang, X., Kong, F., Xue, M., Berner, J., 2016. Impact of a stochastic kinetic energy backscatter scheme on warm season convection-allowing ensemble forecasts. Mon. Wea. Rev. 144, 1887–1908. https://doi.org/10.1175/MWR-D-15-0092.1.

Edwards, R., 2010. Tropical cyclone tornado records for the modernized national weather service era. In: 25th Conf. On Severe Local Storms, P4.1. Amer. Meteor. Soc., Denver, CO. https://ams.confex.com/ams/25SLS/techprogram/paper_175269.htm.

Edwards, R., Dean, A.R., Thompson, R.L., Smith, B.T., 2012. Convective modes for significant severe thunderstorms in the contiguous United States. Part III: tropical cyclone tornadoes. Wea. Forecasting 27, 1507–1519. https://doi.org/10.1175/WAF-D-11-00117.1.

European Centre for Medium-Range Weather Forecasts, 2017. ERA5 reanalysis. Research data archive at the national center for atmospheric research. updated monthly Computational and Information Systems Laboratory. https://doi.org/10.5065/D6X34W69. (Accessed 9 February 2022).

Fujita, T.T., 1977. Anticyclonic tornadoes. Weatherwise 30, 51–64. https://doi.org/10.1080/00431672.1977.9931796.

Gensini, V.A., Brooks, H.E., 2018. Spatial trends in United States tornado frequency. npj Clim. Atmos. Sci. 1, 1–5. https://doi.org/10.1038/s41612-018-0048-2.

Hersbach, H., et al., 2020. The ERA5 global reanalysis. Q. J. R. Meteorol. Soc. 146, 1999–2049. https://doi.org/10.1002/qj.3803.

Hill, E.L., Malkin, W., Schulz Jr., W.A., 1966. Tornadoes associated with cyclones of tropical origin – practical features. J. Appl. Meteor. 5, 745–763. https://www.jstor.org/stable/26173271.

Iacono, M.J., Delamere, J.S., Mlawer, E.J., Shephard, M.W., Clough, S.A., Collins, W.D., 2008. Radiative forcing by long-lived greenhouse Gases: calculations with the AER radiative Transfer models. J. Geophys. Res. 113, D13 https://doi.org/10.1029/2008JD009944.

Janjić, Z.I., 1994. The step-Mountain Eta coordinate model: further developments of the convection, Viscous Sublayer, and Turbulence closure schemes. Mon. Wea. Rev. 122, 927–945. https://doi.org/10.1175/1520-0493(1994)122,0927:TSMECM.2.0.CO;2.

Jung, C., Lackmann, G.M., 2021. The response of extratropical transition of tropical cyclones to climate change: quasi-idealized numerical experiments. J. Clim. 34, 4361–4381. https://doi.org/10.1175/JCLI-D-20-0543.1.

Knutson, T., Camargo, S.J., Chan, J.C.L., Emanuel, K., Ho, C.-H., Kossin, J., Mohapatra, M., Satoh, M., Sugi, M., Walsh, K., Wu, L., 2020. Tropical cyclones and climate change assessment: Part II: projected response to anthropogenic warming. B. of the American. Meteorological Society 101, E303–E322. https://doi.org/10.1175/BAMS-D-18-0194.1.

Landsea, C.W., Franklin, J.L., 2013. Atlantic hurricane Database uncertainty and presentation of a new Database format. Mon. Wea. Rev. 141, 3576–3592.

Li, X., Pu, Z., 2008. Sensitivity of numerical simulation of early rapid intensification of hurricane emily (2005) to cloud microphysical and planetary boundary layer parameterizations. Mon. Wea. Rev. 136, 4819–4838. https://doi.org/10.1175/2008MWR2366.1.

Markowski, P.M., Richardson, Y.P., 2014. The influence of environmental low-level shear and cold pools on tornadogenesis: insights from idealized simulations. J. Atmos. Sci. 71, 243–275. https://doi.org/10.1175/JAS-D-13-0159.1.

McCaul Jr., E.W., 1987. Observations of the hurricane “danny” tornado outbreak of 16 August 1985. Mon. Wea. Rev. 115, 1206–1223. https://doi.org/10.1175/1520-0493(1987)115<1206:OOTHTO>2.0.CO;2.

McCaul Jr., E.W., 1991. Buoyancy and shear characteristics of hurricane-tornado environments. Mon. Wea. Rev. 119, 1954–1978. https://doi.org/10.1175/1520-0493(1991)119<1954:BASCOH>2.0.CO;2.

Meinshausen, M., Nicholls, Z.R.J., Lewis, J., Gidden, M.J., Vogel, E., Freund, M., Beyerle, U., Gessner, C., Nauels, A., Bauer, N., Canadell, J.G., Daniel, J.S., John, A., Krummel, P.B., Luderer, G., Meinshausen, N., Montzka, S.A., Rayner, P.J., Reimann, S., Smith, S.J., van den Berg, M., Velders, G.J.M., Vollmer, M.K., Wang, R. H.J., 2020. The shared socio-economic pathway (SSP) greenhouse gas concentrations and their extensions to 2500. Geosci. Model Dev. (GMD) 13, 3571–3605. https://doi.org/10.5194/gmd-13-3571-2020.

Molinari, J., Vollaro, D., 2008. Extreme helicity and intense convective towers in hurricane bonnie. Mon. Wea. Rev. 136, 4355–4372. https://doi.org/10.1175/2008MWR2423.1.

Moore, T.W., Dixon, R.W., 2011. Climatology of tornadoes associated with Gulf coast-landfalling hurricanes. Geogr. Rev. 101, 371–395. https://www.jstor.org/stable/41303640.

Moore, T.W., Sokol, N.J., Blume, R.A., 2017. Spatial distributions of tropical cyclone tornadoes by intensity and size characteristics. Atmos 8, 1–13. https://doi.org/10.3390/atmos8090160.

Nolan, D.S., McNoldy, B.D., Yunge, J., 2021. Evaluation of the surface wind field over land in WRF simulations of hurricane wilma (2005). Part I: model initialization and simulation validation. Mon. Wea. Rev. 149, 679–695. https://doi.org/10.1175/MWR-D-20-0199.1.

NOAA Global Monitoring Laboratory/Earth System Research Laboratories, 2022. NOAA Solar Calculator. https://gml.noaa.gov/grad/solcalc/. (Accessed 21 September 2023).

NOAA Office for Coastal Management, 2023. Hurricane Costs. https://coast.noaa.gov/states/fast-facts/hurricane-costs.html. (Accessed 18 September 2023).

Novlan, D.J., Gray, W.M., 1974. Hurricane-spawned tornadoes. Mon. Wea. Rev. 102, 476–488. https://doi.org/10.1175/1520-0493(1974)102<0476:HST>2.0.CO;2.

Patricola, C.M., Wehner, M.F., 2018. Anthropogenic influences on major tropical cyclone events. Nature 563, 339–346. https://doi.org/10.1038/s41586-018-0673-2.

Rappaport, E.N., 2014. Fatalities in the United States from atlantic tropical cyclones: new data and interpretation. B. of the American Meteorological Society 95, 341–346. https://doi.org/10.1175/BAMS-D-12-00074.1.

Rasmussen, E.N., 2003. Refined supercell and tornado forecast parameters. Wea. Forecasting 18, 530–535. https://doi.org/10.1175/1520-0434(2003)18<530:RSATFP>2.0.CO;2.

Rasmussen, K.L., Prein, A.F., Rasmussen, R.M., Ikeda, K., Liu, C., 2017. Changes in the convective population and thermodynamic environments in convection-permitting regional climate simulations over the United States. Clim. Dynamics 55, 383–408. https://link.springer.com/article/10.1007/s00382-017-4000-7.

Schär, C., Frei, C., Lüthi, D., Davies, H.C., 1996. Surrogate climate-change scenarios for regional climate models. Geophys. Res. Lett. 23, 669–672. https://doi.org/10.1029/96GL00265.

Schenkel, B.A., Edwards, R., Coniglio, M., 2020. A climatological analysis of ambient deep-tropospheric vertical wind shear impacts upon tornadoes in tropical cyclones. Wea. Forecasting 35, 2033–2059. https://doi.org/10.1175/WAF-D-19-0220.1.

Schenkel, B.A., Coniglio, M., Edwards, R., 2021. How does the relationship between ambient deep-tropospheric vertical wind shear and tropical cyclone tornadoes change between coastal and inland environments? Wea. Forecasting 36, 539–566. https://doi.org/10.1175/WAF-D-20-0127.1.

Schneider, D., Sharp, S., 2007. Radar signatures of tropical cyclone tornadoes in central North Carolina. Wea. Forecasting 22, 278–286. https://doi.org/10.1175/WAF992.1.

Shutts, G., 2005. A kinetic energy backscatter algorithm for use in ensemble prediction systems. Quart. J. Roy. Meteor. Soc. 131, 3079–3102. https://doi.org/10.1256/qj.04.106.

Skamarock, W.C., Klemp, J.B., Dudhia, J., Gill, D.O., Liu, Z., Berner, J., Wang, W., Powers, J.G., Duda, M.G., Barker, D.M., Huang, X.-Y., 2021. A description of the advanced research WRF version 4.3. NCAR Tech. Note NCAR/TN-556+STR 145. https://doi.org/10.5065/1dfh-6p97.

Spratt, S.M., Sharp, D.W., Welsh, P., Sandrik, A., Alsheimer, F., Paxton, C., 1997. A WSR-88d assessment of tropical cyclone outer rainband tornadoes. Wea. and Forecasting 12, 479–501. https://doi.org/10.1175/1520-0434(1997)012<0479:AWAOTC>2.0.CO;2.

Thompson, G., Field, P.R., Rasmussen, R.M., Hall, W.D., 2008. Explicit forecasts of winter precipitation using an improved bulk microphysics scheme. Part II: implementation of a new snow parameterization. Mon. Wea. Rev. 136, 5095–5115. https://doi.org/10.1175/2008MWR2387.1.

Thompson, L.R., Edwards, R., Mead, C.R., 2004. An update to the supercell composite and significant tornado parameters. In: *22nd Conf. On Severe Local Storms*, Hyannis, MA, Amer. Meteor. Soc., CD-ROM, P8.1.

Thompson, R.L., Edwards, R., Hart, J.A., Elmore, K.L., Markowski, P., 2003. Close proximity soundings within supercell environments obtained from the rapid update cycle. Wea. Forecasting 18, 1243–1261. https://doi.org/10.1175/1520-0434(2003)018<1243:CPSWSE>2.0.CO;2.

Trapp, R.J., Hoogewind, K.A., 2016. The realization of extreme tornadic storm events under future anthropogenic climate change. J. Clim. 29, 5251–5265. https://doi.org/10.1175/JCLI-D-15-0623.1.

The University of Melbourne, 2020. Greenhouse Gas Concentrations – Greenhouse Gas Factsheets. https://greenhousegases.science.unimelb.edu.au/#!/view. (Accessed 20 February 2023).